JACS
JOURNAL OF THE AMERICAN CHEMICAL SOCIETY

Communication

pubs.acs.org/JACS

Water Oxidation by an Electropolymerized Catalyst on Derivatized Mesoporous Metal Oxide Electrodes

Dennis L. Ashford,[†] Alexander M. Lapides,[†] Aaron K. Vannucci, Kenneth Hanson, Daniel A. Torelli, Daniel P. Harrison, Joseph L. Templeton,* and Thomas J. Meyer*

Department of Chemistry, University of North Carolina at Chapel Hill, CB 3290, Chapel Hill, North Carolina 27599, United States

Supporting Information

ABSTRACT: A general electropolymerization/electro-oligomerization strategy is described for preparing spatially controlled, multicomponent films and surface assemblies having both light harvesting chromophores and water oxidation catalysts on metal oxide electrodes for applications in dye-sensitized photoelectrosynthesis cells (DSPECs). The chromophore/catalyst ratio is controlled by the number of reductive electrochemical cycles. Catalytic rate constants for water oxidation by the polymer films are similar to those for the phosphonated molecular catalyst on metal oxide electrodes, indicating that the physical properties of the catalysts are not significantly altered in the polymer films. Controlled potential electrolysis shows sustained water oxidation over multiple hours with no decrease in the catalytic current.

Dye-sensitized photoelectrosynthesis cells (DSPECs) offer a potential solution to solar energy storage by using solar energy to directly generate chemical fuels.[1,2] In a DSPEC, the configuration of the chromophore and catalyst is important in enabling rapid electron transfer from the catalyst to the oxidized chromophore following the excitation-electron injection sequence.[3,4]

Multiple strategies have been described for assembling chromophores and catalysts on metal oxide surfaces.[5−12] They typically suffer from difficult synthetic procedures and/or limited stabilities on oxide surfaces.[13,14] Recently, we reported reductive electropolymerization/electro-oligomerization of a vinyl-functionalized polypyridyl complex, $[Fe(4'\text{-vinyl-}2,2':6',2''\text{-terpyridine})_2]^{2+}$, on bare TiO_2 and on TiO_2 surfaces prederivatized with the vinyl- and phosphonate-functionalized complex, $[Ru(dvb)_2((PO_3H_2)_2bpy)]^{2+}$ (**RuPdvb**$^{2+}$; dvb = 5,5′-divinyl-2,2′-bipyridine; $(PO_3H_2)_2bpy$ = [2,2′-bipyridine]-4,4′-diylbis(phosphonic acid)).[15,16] The effect of adding the electropolymerized overlayer is dramatic, leading to a 30-fold enhancement in photostability of the surface-bound chromophore relative to the unprotected complex.

Here we describe utilization of this strategy to introduce the vinyl-functionalized water oxidation catalyst, $[Ru(Mebimpy)(dvb)(OH_2)]^{2+}$ (**RuOH$_2$**$^{2+}$, Mebimpy = 2,6-bis(1-methyl-1*H*-benzo[*d*]imidazole-2-yl)pyridine), as the electropolymerized overlayer (Figure 1). This procedure provides a basis for preparing stable, catalytically active films both with and without the prebound **RuPdvb**$^{2+}$ chromophore on both planar oxide surfaces and in mesoporous, nanoparticle metal oxide films.

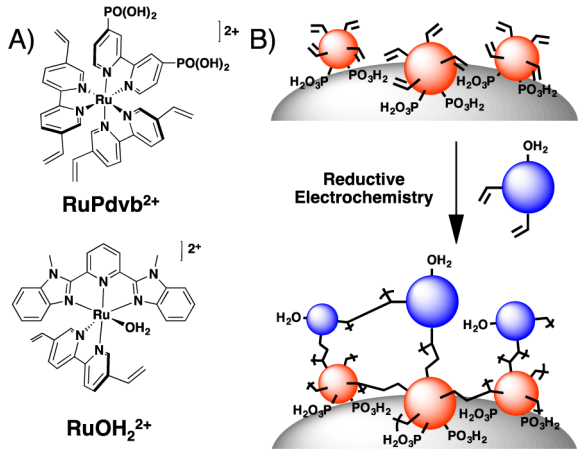

Figure 1. (A) Structures of **RuPdvb**$^{2+}$ and **RuOH$_2$**$^{2+}$. (B) Schematic diagram of the surface structure following reductive electropolymerization of **RuOH$_2$**$^{2+}$ on *n*TiO_2-**RuPdvb**$^{2+}$.

The chromophore, **RuPdvb**$^{2+}$, and catalyst, **RuOH$_2$**$^{2+}$, were synthesized as previously reported (see Supporting Information (SI)).[5,15] Substitution of coordinated H_2O by CH_3CN was achieved by dissolving **RuOH$_2$**$^{2+}$ in CH_3CN. Vapor diffusion of diethyl ether resulted in X-ray quality crystals of the CH_3CN-substituted complex (Figure S1). In the structure, the geometry around Ru(II) is a slightly distorted octahedron with bond angles of 174.2° for N1−Ru−N3 and 174.4° for N2−Ru−N6. The length of the vinyl C−C bonds (1.30 Å) and the Ru−N bonds match those of similar complexes.[17]

Electropolymerization was conducted in a three-compartment electrochemical cell under an argon atmosphere. All solutions were dried over $MgSO_4$, filtered, and deaerated with argon for 10 min before electropolymerization. The working electrodes were planar fluoride-doped tin oxide (*p*FTO), nanocrystalline titanium dioxide (*n*TiO_2), or nanocrystalline indium tin oxide (*n*ITO). Working electrodes were either the bare metal oxide or derivatized with **RuPdvb**$^{2+}$ by soaking overnight in methanol solutions of the complex (150 μM).[15] In a typical electropolymerization experiment, the working electrode was cycled in a solution of **RuOH$_2$**$^{2+}$ (0.5 mM in complex, 0.1 M $TBAPF_6$/PC; PC = propylene carbonate) from 0 to −1.8 V (vs $Ag/AgNO_3$) at a scan rate of 100 mV s^{-1} with a 120 s pause between each cycle. PC was used as the

Received: March 11, 2014
Published: April 15, 2014

   dx.doi.org/10.1021/ja502464s | *J. Am. Chem. Soc.* 2014, 136, 6578−6581

electrochemical solvent rather than CH_3CN to avoid displacing the H_2O ligand of **RuOH$_2^{2+}$**. Solutions were stirred during and between cycles to promote percolation of **RuOH$_2^{2+}$** throughout the mesoporous metal oxides (*n*ITO and *n*TiO_2).[15]

Initially, electropolymerization was carried out on *p*FTO electrodes and on *p*FTO derivatized with **RuPdvb^{2+}** (*p*FTO-**RuPdvb^{2+}**). Surface coverages (Γ) of polymerized **RuOH$_2^{2+}$** on *p*FTO (*poly***RuOH$_2^{2+}$**) were determined by cyclic voltammetry (CV). In these measurements, the charge passed under the $Ru^{III/II}$ wave (Figure S17A), and the expression in eq S1, were used to establish Γ in mol cm^2. Surface coverages on *p*FTO-*poly***RuOH$_2^{2+}$** and *p*FTO-**RuPdvb^{2+}**-*poly***RuOH$_2^{2+}$** increased linearly with the number of reductive scan cycles (Figure S2). Under the electropolymerization conditions, one monolayer equivalent (~1×10^{-10} mol cm^{-2} on planar surfaces) of *poly***RuOH$_2^{2+}$** was deposited every ~2 cycles on both *p*FTO and *p*FTO-**RuPdvb^{2+}**. The peak current (i_p) for the *poly*$Ru^{III/II}OH_2^{3+/2+}$ couple in aqueous 0.1 M $HClO_4$ varied linearly with scan rate for *p*FTO-**RuPdvb^{2+}**-*poly***RuOH$_2^{2+}$** with both 5 and 20 layers of *poly***RuOH$_2^{2+}$** (Figure S3), consistent with a nondiffusional surface redox couple.[18]

The pH-dependence of the *poly*$Ru^{III/II}OH_2^{3+/2+}$ couple on *p*FTO is illustrated in the $E_{1/2}$ vs pH (Pourbaix) diagram in Figure 2. Below pH 2.3, the couple is pH independent. Above

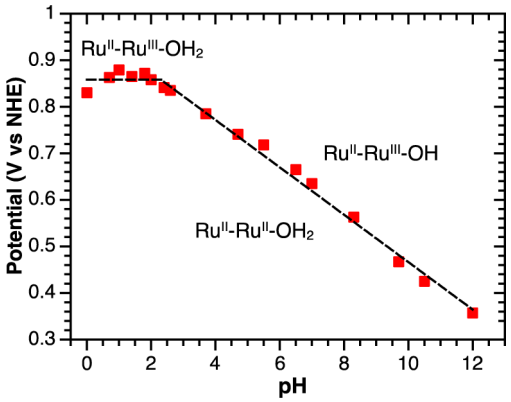

Figure 2. $E_{1/2}$ vs pH diagram for *p*FTO-**RuPdvb^{2+}**-*poly***RuOH$_2^{2+}$** (five layers). $E_{1/2}$ values are cited as potentials at the current maxima in square wave voltammograms. The dashed lines are the fit for the $E_{1/2}$–pH trends for the couples *poly*$Ru^{III}OH_2^{3+}/Ru^{II}OH_2^{2+}$ (~0 mV/pH unit) and *poly*$Ru^{III}OH^{2+}/Ru^{II}OH_2^{2+}$ (51 mV/pH unit) with pK_a = 2.3 for *poly*$Ru^{III}OH_2^{3+}$ at 23 °C in aqueous 0.5 M $NaClO_4$ with 0.1 M buffer.

pH 2.3, $E_{1/2}$ decreases by 51 mV/pH unit, suggesting that pK_a = 2.3 for *poly*$Ru^{III}OH_2^{3+}$. This value is comparable to that of the surface bound catalyst [Ru(Mebimpy)(4,4′-$(PO_3H_2$-$CH_2)_2$-bpy)$(OH_2)]^{2+}$ (**RuPOH$_2^{2+}$**: 4,4′-$(PO_3H_2$-$CH_2)_2$-bpy = ([2,2′-bipyridine]-4,4′-diylbis(methylene))bis(phosphonic acid)) on *n*TiO_2 (pK_a = 2.5).[19] The ensuing *poly*$Ru^{IV}O^{2+}/Ru^{III}OH^{2+}$ couple is kinetically inhibited and difficult to observe, as documented earlier for related ruthenium complexes.[20] The electrochemical response of the couples is independent of film thickness in *p*FTO-*poly***RuOH$_2^{2+}$** in films up to 33 layers (Figure S4). These results suggest that the environment at the Ru(II) metal centers in *poly***RuOH$_2^{2+}$** is open to diffusion of solvent and buffer/electrolyte through the polymer, at least to this level of thickness.

Electropolymerization was also investigated on *n*TiO_2 and *n*TiO_2-**RuPdvb^{2+}** electrodes (4–7 μm thick). The high surface area electrodes allow for UV/visible monitoring of surface coverage based on λ_{max} = 497 nm, $\varepsilon_{497\ nm}$ = 8200 M^{-1} cm^{-1} for *poly***RuOH$_2^{2+}$**. On both surfaces, surface coverage of *poly*-**Ru^{II}OH$_2^{2+}$** increased linearly with the number of scans (Figures 3 and S6) for the first 50 reductive cycles. With additional

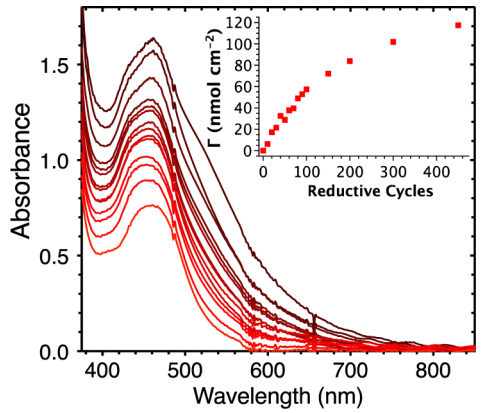

Figure 3. UV/visible spectral changes for *n*TiO_2-**RuPdvb^{2+}** with an increasing number of reductive scan cycles (0, 10, 20, 30, 40, 50, 60, 70, 80, 90, 100, 150, 200, 300, 450; light red to dark red) in 0.5 mM **RuOH$_2^{2+}$** (0.1 M $TBAPF_6$/PC). Inset: Surface coverage (Γ) of *poly***RuOH$_2^{2+}$** versus the number of reductive scan cycles.

scans, surface coverage continues to increase, but at a slower rate with a plateau reached after ~300 cycles. Surface coverages following 70 and 300 cycles correspond to one (Γ ≈ 7×10^{-8} mol cm^{-2} on *n*TiO_2) and two layers of *poly***Ru^{II}OH$_2^{2+}$**, respectively.

A blue shift in the MLCT absorption maximum from 462 to 453 nm is observed for **RuPdvb^{2+}** in the electropolymerized films (Figures 3, S7). This shift is consistent with conversion of the π* acceptor vinyl substituents in **RuPdvb^{2+}** to saturated, electron-donating alkyl substituents in the electropolymerized polymers.[15] This observation suggests the formation of direct C–C bonds between surface-bound **RuPdvb^{2+}** and catalyst **RuOH$_2^{2+}$** in the surface assembly.[15,21] No change in the absorption spectrum of *n*TiO_2-**RuPdvb^{2+}** was observed following reductive cycling in the absence of **RuOH$_2^{2+}$**.

Scanning electron microscopy (SEM) images of *n*TiO_2-**RuPdvb^{2+}**-*poly***RuOH$_2^{2+}$** films following 60 reductive CVs show that the *n*TiO_2 films maintain their porosity (Figure S8). A decrease in porosity is observed following 120 reductive cycles. Following 450 reductive cycles, a film of *poly***RuOH$_2^{2+}$** is visible on top of the *n*TiO_2 substrate. Film formation presumably inhibits diffusion into the pores of the mesoporous oxide, inhibiting further internal polymerization (Figure 3). Energy-dispersive X-ray spectroscopy (EDS) was used to determine the concentration of Ru at varying depths following 450 reductive scans (Figure S9). These results suggest a relatively uniform concentration of Ru throughout the *n*TiO_2 substrate.

The photostability of the *n*TiO_2-**RuPdvb^{2+}**-*poly***RuOH$_2^{2+}$** films was evaluated by a previously published procedure in which the derivatized electrodes were subjected to constant irradiation at 455 nm (fwhm ~30 nm, 475 mW/cm^2, ~135 suns at 455 nm).[22] Absorption spectra (360–800 nm) of the films were obtained every 15 min over 16 h of irradiation. Results for 1:1 *n*TiO_2-**RuPdvb^{2+}**-*poly***RuOH$_2^{2+}$** in aqueous 0.1 M $HClO_4$ demonstrate significant enhancements in surface stability compared to *n*TiO_2-**RuP^{2+}** (**RuP^{2+}** = Ru(bpy)$_2$($(PO_3H_2)_2$bpy)$]^{2+}$, Figure S10). Following 16 h of

dx.doi.org/10.1021/ja502464s | J. Am. Chem. Soc. 2014, 136, 6578–6581

irradiation, the surface coverage of the chromophore in nTiO$_2$-**RuP**$^{2+}$ decreased by ~70% while only ~10% was lost for nTiO$_2$-**RuPdvb**$^{2+}$-*poly***RuOH**$_2^{2+}$ (Figure 4). A 15-fold enhancement of stability was observed for nTiO$_2$-**RuPdvb**$^{2+}$-*poly*-**RuOH**$_2^{2+}$ films (k_{des} = 2.8 × 10^{-5} s^{-1}; k_{des} is the rate constant for loss of the chromophore from the surface) compared to nTiO$_2$-**RuP**$^{2+}$ (k_{des} > 30 × 10^{-5} s^{-1}) at pH 4.7 (0.1 M NaOAc/HOAc and 0.5 M NaClO$_4$), Figure S11.[14,15,22]

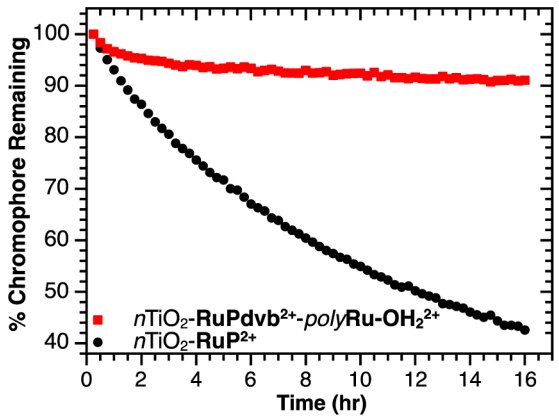

Figure 4. Variation of surface coverage as a function of irradiation time at 475 mW/cm^2 at 455 nm over a 16 h photolysis period in aqueous 0.1 M HClO$_4$. Loss from the surfaces was monitored by absorbance changes at 453 nm (ε_{453} = 13 500 M^{-1} cm^{-1}) which were also corrected for light scattering from TiO$_2$.

Electrocatalytic water oxidation was investigated on nITO-**RuPdvb**$^{2+}$-*poly***RuOH**$_2^{2+}$ by CV measurements. At pH 4.7 (0.1 M NaOAc/HOAc, 0.5 M NaClO$_4$) oxidative waves appear at $E_{1/2}$ = 0.75 and 1.02 V (vs NHE) for the $-(Ru^{II})^{2+}-(Ru^{III}-OH)^{2+}/-(Ru^{II})^{2+}-(Ru^{II}-OH_2)^{2+}$ and $-(Ru^{II})^{2+}-(Ru^{IV}=O)^{2+}/-(Ru^{II})^{2+}-(Ru^{III}-OH)^{2+}$ couples, respectively (Figure 5). An additional wave appears at $E_{1/2}$ = 1.38 V for the

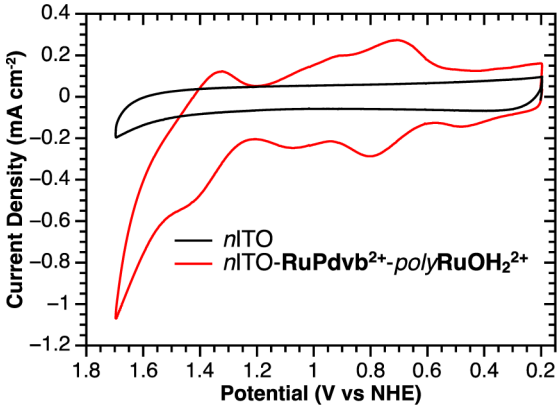

Figure 5. Cyclic voltammograms at 20 mV/s for nITO-**RuPdvb**$^{2+}$-*poly***RuOH**$_2^{2+}$ (red) and nITO (black) in pH 4.7 aqueous solution (0.1 M NaOAc/HOAc, 0.5 M NaClO$_4$); Pt-mesh counter electrode and Ag/AgCl reference electrode, 0.197 V vs NHE.

$-(Ru^{III})^{3+}-(Ru^{IV}=O)^{2+}/-(Ru^{II})^{2+}-(Ru^{IV}=O)^{2+}$ redox couple. Spectroelectrochemical measurements on nITO-**RuPdvb**$^{2+}$-*poly***RuOH**$_2^{2+}$ in aqueous 0.1 M HClO$_4$ are consistent with the loss of MLCT absorptions in the visible and with other characteristic spectral changes following oxidation of $-(Ru^{II})^{2+}-(Ru^{II}-OH_2)^{2+}$ to $-(Ru^{II})^{2+}-(Ru^{III}-OH_2)^{3+}$, $-(Ru^{II})^{2+}-(Ru^{III}-OH_2)^{3+}$ to $-(Ru^{II})^{2+}-(Ru^{IV}=O)^{2+}$, and $-(Ru^{II})^{2+}-(Ru^{IV}=O)^{2+}$ to $-(Ru^{III})^{3+}-(Ru^{IV}=O)^{2+}$ (Figure S12).

As shown in Figure 5, oxidation past the $-(Ru^{III})^{3+}-(Ru^{IV}=O)^{2+}/-(Ru^{II})^{2+}-(Ru^{IV}=O)^{2+}$ couple triggers the onset of catalytic water oxidation. Notably, it occurs at a potential ~200 mV less positive than oxidation to $-(Ru^{III})^{3+}-(Ru^{V}(O))^{3+}$ which occurs at $E_{p,a}$ ~1.7 V for the solution-based catalyst.[23] The $-(Ru^{III})^{3+}-(Ru^{V}(O))^{3+}/-(Ru^{III})^{3+}-(Ru^{IV}=O)^{2+}$ wave in the bilayer is not observable due to the catalytic current. The appearance of the low potential onset suggests that the chromophore **RuPdvb**$^{2+}$ in the films behaves as a redox mediator, lowering the overpotential for water oxidation.[24−26] A similar decrease was not observed for *poly***RuOH**$_2^{2+}$ films on nITO (Figure S13).

Rate constants for water oxidation (k_{obs}) at 1.7 V (vs NHE) were evaluated at pH 4.7 (0.1 M NaOAc/HOAc, 0.5 M NaClO$_4$) by CV measurements with application of eq S2 (see SI).[20] Based on these data, k_{obs} = 0.073 ± 0.030 s^{-1} for nITO-**RuPdvb**$^{2+}$-*poly***RuOH**$_2^{2+}$ with a 1:1 chromophore/catalyst ratio and k_{obs} = 0.060 ± 0.020 s^{-1} for nTiO$_2$-*poly***RuOH**$_2^{2+}$ (Figure S14). Under the same conditions, k_{obs} = 0.10 ± 0.010 s^{-1}, for the monomeric catalyst **RuPOH**$_2^{2+}$ on nITO (Figure S14). The comparable k_{obs} suggests that the catalytic properties of the catalyst are not significantly altered in the polymer film. Similar k_{obs} values were obtained on pFTO (Figure S15).

Controlled potential electrolysis of 1:1 nITO-**RuPdvb**$^{2+}$-*poly***RuOH**$_2^{2+}$ at 1.7 V (vs NHE) in pH 4.7 (0.1 M NaOAc/HOAc, 0.5 M NaClO$_4$, $E°(H_2O \rightarrow 1/2\ O_2 + 2\ H^+ + 2\ e^-)$ = 0.95 V vs NHE at pH 4.7) resulted in a sustained catalytic current with no decrease over a 2 h period (Figure 6). Oxygen

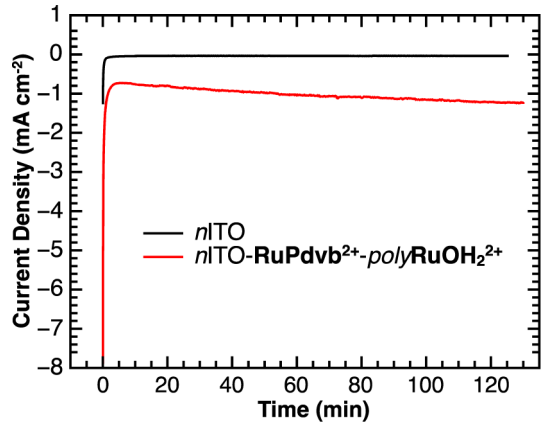

Figure 6. Controlled potential electrolysis on 1:1 nITO-**RuPdvb**$^{2+}$-*poly***RuOH**$_2^{2+}$ (red) and nITO (black) at 1.7 V (vs NHE) in pH 4.7 aqueous solution (0.1 M NaOAc/HOAc, 0.5 M NaClO$_4$); Pt-mesh counter electrode and Ag/AgCl reference electrode with $\Gamma \approx 1.1 \times 10^{-8}$ mol cm^{-2} for both complexes.

production was quantified by gas chromatography, giving a Faradaic efficiency of 77% (Figure S16). During this experiment, the catalytic sites underwent 501 turnovers with a turnover frequency of 0.046 s^{-1} (based on oxygen production), comparable to the rate constants obtained by CV measurements.

Following a 2 h electrolysis period, neither catalyst decomposition nor desorption was observed by CV (Figure S17). This represents a significant stability enhancement relative to surface-bound **RuPOH**$_2^{2+}$. These measurements

dx.doi.org/10.1021/ja502464s | J. Am. Chem. Soc. 2014, 136, 6578−6581

reveal a chemical change for surface-bound $\mathbf{RuPdvb}^{2+}$ over the electrolysis period with characteristic features appearing in the CVs for a surface-bound analogue of *cis*-$[Ru(bpy)_2(OH_2)_2]^{2+}$.[19] Its appearance and activity toward water oxidation catalysis may account for the increase in the magnitude of the catalytic current over time observed during electrolysis (Figure 6).

Our results are important in describing a general strategy for preparing spatially controlled, multicomponent films and bilayers containing both light harvesting chromophores and water oxidation catalysts on planar and mesoporous nanoparticle metal oxide films. The procedure is general with reductive electropolymerization/assembly formation successfully demonstrated on *p*FTO, *n*TiO_2, and *n*ITO and on these surfaces derivatized with $\mathbf{RuPdvb}^{2+}$. The chromophore/catalyst ratio in the films can be controlled by the number of reductive CVs scan cycles. The PCET character of the $\mathbf{RuOH_2}^{2+}$ sites in the surface structures is maintained and, on *p*FTO, is independent of film thickness up to 33 layers. Importantly, reactivity toward water oxidation is maintained in both *poly*$\mathbf{RuOH_2}^{2+}$ films and $\mathbf{RuPdvb}^{2+}$-*poly*$\mathbf{RuOH_2}^{2+}$ bilayers on *p*FTO and *n*ITO with sustained water oxidation catalysis occurring over a 2 h electrolysis period with a Faradaic efficiency of 77% with individual catalyst sites undergoing 501 turnovers and a TOF = 0.046 s^{-1}.

■ ASSOCIATED CONTENT

Supporting Information

Detailed experimental procedures and EDS analysis, UV/vis absorption spectra, crystal structure, and electrochemical characterizations. This material is available free of charge via the Internet at http://pubs.acs.org.

■ AUTHOR INFORMATION

Corresponding Authors

joetemp@unc.edu
tjmeyer@unc.edu

Author Contributions

†D.L.A. and A.M.L. contributed equally.

Notes

The authors declare no competing financial interest.

■ ACKNOWLEDGMENTS

This research was supported by the UNC EFRC Center for Solar Fuels, an Energy Frontier Research Center funded by the U.S. Department of Energy, Office of Science, Office of Basic Energy Sciences, under Award No. DE-SC0001011, supporting A.K.V. and K.H. D.L.A. acknowledges support from the Department of Energy Office of Science Graduate Fellowship Program under Contract No. DE-AC05-06OR23100. A.M.L. acknowledges Government support under FA9550-11-C-0028 and awarded by the DOD, AFOSR, NDSEG Fellowship, 32 CFR 168a. Support is also acknowledged by D.P.H. from the U.S. Department of Energy, Office of Science, Office of Basic Energy Sciences, under Award Number DE-FG02-06ER15788.

■ REFERENCES

(1) Gratzel, M. *Nature* **2001**, *414*, 338.
(2) Lewis, N. S.; Nocera, D. G. *Proc. Natl. Acad. Sci. U.S.A.* **2006**, *103*, 15729.
(3) Swierk, J. R.; Mallouk, T. E. *Chem. Soc. Rev.* **2013**, *42*, 2357.
(4) Young, K. J.; Martini, L. A.; Milot, R. L.; Snoeberger, R. C.; Batista, V. S.; Schmuttenmaer, C. A.; Crabtree, R. H.; Brudvig, G. W. *Coord. Chem. Rev.* **2012**, *256*, 2503.
(5) Ashford, D. L.; Song, W. J.; Concepcion, J. J.; Glasson, C. R. K.; Brennaman, M. K.; Norris, M. R.; Fang, Z.; Templeton, J. L.; Meyer, T. J. *J. Am. Chem. Soc.* **2012**, *134*, 19189.
(6) Concepcion, J. J.; Jurss, J. W.; Hoertz, P. G.; Meyer, T. J. *Angew. Chem., Int. Ed.* **2009**, *48*, 9473.
(7) Hanson, K.; Torelli, D. A.; Vannucci, A. K.; Brennaman, M. K.; Luo, H.; Alibabaei, L.; Song, W.; Ashford, D. L.; Norris, M. R.; Glasson, C. R. K.; Concepcion, J. J.; Meyer, T. J. *Angew. Chem., Int. Ed.* **2012**, *51*, 12782.
(8) Glasson, C. R. K.; Song, W.; Ashford, D. L.; Vannucci, A.; Chen, Z.; Concepcion, J. J.; Holland, P. L.; Meyer, T. J. *Inorg. Chem.* **2012**, *51*, 8637.
(9) Xiang, X.; Fielden, J.; Rodriguez-Cordoba, W.; Huang, Z.; Zhang, N.; Luo, Z.; Musaev, D. G.; Lian, T.; Hill, C. L. *J. Phys. Chem. C* **2013**, *117*, 918.
(10) Gao, Y.; Ding, X.; Liu, J.; Wang, L.; Lu, Z.; Li, L.; Sun, L. *J. Am. Chem. Soc.* **2013**, *135*, 4219.
(11) Moore, G. F.; Blakemore, J. D.; Milot, R. L.; Hull, J. F.; Song, H.-e.; Cai, L.; Schmuttenmaer, C. A.; Crabtree, R. H.; Brudvig, G. W. *Energy Environ. Sci.* **2011**, *4*, 2389.
(12) Mola, J.; Mas-Marza, E.; Sala, X.; Romero, I.; Rodriguez, M.; Vinas, C.; Parella, T.; Llobet, A. *Angew. Chem., Int. Ed.* **2008**, *47*, 5830.
(13) Frischmann, P. D.; Mahata, K.; Wuerthner, F. *Chem. Soc. Rev.* **2013**, *42*, 1847.
(14) Hanson, K.; Brennaman, M. K.; Luo, H.; Glasson, C. R. K.; Concepcion, J. J.; Song, W.; Meyer, T. J. *ACS Appl. Mater. Interfaces* **2012**, *4*, 1462.
(15) Lapides, A. M.; Ashford, D. L.; Hanson, K.; Torelli, D. A.; Templeton, J. L.; Meyer, T. J. *J. Am. Chem. Soc.* **2013**, *135*, 15450.
(16) Moss, J. A.; Yang, J. C.; Stipkala, J. M.; Wen, X.; Bignozzi, C. A.; Meyer, G. J.; Meyer, T. J. *Inorg. Chem.* **2004**, *43*, 1784.
(17) Biner, M.; Buergi, H. B.; Ludi, A.; Roehr, C. *J. Am. Chem. Soc.* **1992**, *114*, 5197.
(18) Bard, A. J.; Faulkner, L. R. *Electrochemical Methods: Fundamentals and Applications*, 2nd ed.; Wiley: New York, 2001.
(19) Song, W.; Ito, A.; Binstead, R. A.; Hanson, K.; Luo, H.; Brennaman, M. K.; Concepcion, J. J.; Meyer, T. J. *J. Am. Chem. Soc.* **2013**, *135*, 11587.
(20) Vannucci, A. K.; Hull, J. F.; Chen, Z.; Binstead, R. A.; Concepcion, J. J.; Meyer, T. J. *J. Am. Chem. Soc.* **2012**, *134*, 3972.
(21) Calvert, J. M.; Schmehl, R. H.; Sullivan, B. P.; Facci, J. S.; Meyer, T. J.; Murray, R. W. *Inorg. Chem.* **1983**, *22*, 2151.
(22) Hanson, K.; Losego, M. D.; Kalanyan, B.; Ashford, D. L.; Parsons, G. N.; Meyer, T. J. *Chem. Mater.* **2013**, *25*, 3.
(23) Concepcion, J. J.; Jurss, J. W.; Norris, M. R.; Chen, Z. F.; Templeton, J. L.; Meyer, T. J. *Inorg. Chem.* **2010**, *49*, 1277.
(24) Concepcion, J. J.; Jurss, J. W.; Templeton, J. L.; Meyer, T. J. *Proc. Natl. Acad. Sci. U.S.A.* **2008**, *105*, 17632.
(25) Norris, M. R.; Concepcion, J. J.; Harrison, D. P.; Ashford, D. L.; Fang, Z.; Binstead, R. A.; Templeton, J. L.; Meyer, T. J. *J. Am. Chem. Soc.* **2013**, *135*, 2080.
(26) Norris, M. R.; Concepcion, J. J.; Fang, Z.; Templeton, J. L.; Meyer, T. J. *Angew. Chem., Int. Ed.* **2013**, *52*, 13580.